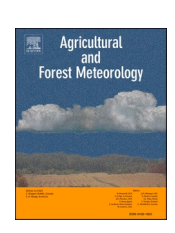
ELSEVIER

Contents lists available at ScienceDirect

Agricultural and Forest Meteorology

journal homepage: www.elsevier.com/locate/agrformet





Biophysical effects of paddy rice expansion on land surface temperature in Northeastern Asia

Wenqi Liu^{a,b}, Jinwei Dong^{a,*}, Guoming Du^c, Geli Zhang^d, Zhixin Hao^a, Nanshan You^a, Guosong Zhao^e, K. Colton Flynn^f, Tong Yang^d, Yuting Zhou^{b,*}

- ^a Key Laboratory of Land Surface Pattern and Simulation, Institute of Geographic Sciences and Natural Resources Research, Chinese Academy of Sciences, Beijing 100101. China
- ^b Department of Geography, Oklahoma State University, Stillwater, OK 74075, USA
- ^c School of Public Administration and Law, Northeast Agricultural University, Harbin 150030, China
- ^d College of Land Science and Technology, China Agricultural University, Beijing 100083, China
- ^e Key Laboratory of Regional Ecology and Environmental Change, School of Geography and Information Engineering, China University of Geosciences, Wuhan 430074, China
- f USDA-ARS, Grassland Soil and Water Research Laboratory, Temple, TX 76502, USA

ARTICLE INFO

Keywords: Rice expansion Land use change LST Biophysical effects Surface energy balance

ABSTRACT

The pending extensive rice expansion in northeastern Asia, especially in northeast China, affects regional climate by altering both biogeochemical and biophysical processes. While the biogeochemical effects (e.g., CO₂, CH₄) of rice expansion have attracted plenty of attention, its biophysical effects have not been well documented, especially its influences on diurnal and seasonal land surface temperature (LST). In this study, we used a pair-wise comparison approach to examine biophysical effects of paddy rice expansion at different temporal scales (diurnal and seasonal) in northeast China, based on satellite-derived biophysical proxies and a high-resolution crop map in 2017. We found that the daily mean LST of rice paddies was 0.5 °C lower than that of corn and soybean fields during the growing season (from May to September), as a result of daytime cooling (-1.8 and -2.0 $^{\circ}\text{C})$ and nighttime warming (0.8 and 1.1 $^{\circ}\text{C})$, which subsequently led to a narrower diurnal LST range (-2.6 and -3.0 °C) than in upland crops (i.e. corn and soybean). The cooling effects were stronger in the early period of the growing season (May and June) than in the late season (July to September). Using a temperature response model, we found that the nonradiative processes (i.e., evapotranspiration and sensible heat) dominated the LST response in paddy rice, while the radiative process (i.e., albedo) played a secondary role. The daytime cooling and nighttime warming implies that we need to consider the unsymmetrical diurnal LST dynamics when evaluating the short-term effects of paddy rice expansion. Stronger cooling effects in the early growing season has to be accounted for when modeling its biophysical impacts at seasonal scale. This study explained the local climate effects of rice expansion through the biophysical mechanism with both radiative and nonradiative controls on the surface energy balance, which can contribute to improved modeling of biophysical effects of land use change.

1. Introduction

Anthropogenic land use change plays a critical role in climate change processes and mitigation (Zhou et al., 2016; IPCC, 2019; Yu et al., 2020a; Zhou et al., 2020). In recent decades, a remarkable paddy rice expansion in the high latitudes of northeastern Asia has received much attention (Liu et al., 2010; Dong et al., 2015, 2016). One hotspot of paddy rice expansion in this region is northeast China (Wang et al., 2011; Shi et al., 2013; Zhang et al., 2017). Considerable upland crop

(mainly corn and soybean) fields have been converted into rice paddies, causing an increase of paddy rice area in the region by 3.68 million ha from 2000 to 2017 (Xin et al., 2020), which makes the region known as China's new rice bowl. This unprecedented expansion of paddy rice on upland crops has significant ecological, environmental, and climatic consequences, but has been rarely examined in detail (Fu et al., 2020; Luo et al., 2020; Singha et al., 2020).

Land use changes alter both biogeochemical factors (e.g., carbon stocks and greenhouse gas emissions) and energy partitioning (e.g.,

E-mail addresses: dongjw@igsnrr.ac.cn (J. Dong), yuting.zhou@okstate.edu (Y. Zhou).

^{*} Corresponding authors.

albedo and evapotranspiration) (Peng et al., 2017; Elias et al., 2020; Huang et al., 2020). Numerous studies have revealed effects of land conversion on the biogeochemical process, for example, afforestation and conservation of forests significantly increase carbon uptake (Huang et al. 2018a; Windisch et al., 2021) while expansion of wetlands increases CO₂ and CH₄ emissions rapidly (Wei and Wang, 2017; Hemes et al., 2018). At the local and regional scale, biophysical factors could play an important role in affecting temperature in comparison to solely biogeochemical factors (Peng et al., 2014; Zhao and Jackson, 2016). However, to date, the climate effects of land use change, for example paddy rice expansion, mainly focus on the biogeochemical processes manifested as greenhouse gas emissions (Xu et al., 2011; (Liu et al., 2019c); Hwang et al., 2020), while few studies have investigated its biophysical processes.

The underlying biophysical impact of land use change on climate has been mostly unraveled for certain land use types including afforestation, global greening, and wetland reclamation (Cao et al., 2019; (Liu et al., 2019d); Prevedello et al., 2019; Chen et al., 2020; Jin et al., 2020; Wang et al., 2020; Yuan et al., 2020). In these studies, biophysical impacts, generally measured in land surface temperature (LST), were mainly affected by variations of surface physical characteristics (such as leaf area index, turbulent flux, soil moisture, etc.). However, variations of biophysical indicators caused by conversion from upland crops to paddy rice have not been fully examined yet, despite a considerable paddy rice expansion in northeast China (Xin et al., 2020). Similar to flooded fields with low vegetation cover, paddy rice fields are regarded as a type of artificial wetlands (Yu and Liu 2019). The energy exchange of paddy rice fields is thus similar to that of wetlands (Liu et al., 2019a; Nocco et al., 2019). Shen et al. (2020) showed that the loss of marshlands and forests increased local LST by altering local albedo and evapotranspiration (ET). The two types of conversions, from marshland to paddy rice and from marshland to upland field crops, were found to have different effects on LST. Moreover, the conversion from upland field crops to paddy rice decreased the LST, resembling the cooling effects of wetlands ((Liu et al., 2019b)).

Remote sensing observations and surface energy models are powerful tools for investigating biophysical changes caused by land use change. Some studies explored redistribution of surface energy caused by land cover change using site-level meteorological data, which often suffer in spatial discontinuity compared to those incorporating remote sensing data (Huang et al. 2018b; Nocco et al., 2019). However, even with continuous data from remote sensing, studies encompassing multi-year analyses usually do not discriminate the contributions of land use change from the effects caused by interannual climate dynamics, also termed as climate background (Pan et al., 2020). The pair-wise comparison approach (Wang et al., 2018; Abera et al., 2020) or the "Observation Minus Reanalysis" approach (Kalnay and Cai 2003) can separate the effects from land use change and climate background and have been widely used to quantify the relative contribution of land use change. However, it has not been applied in the impact analyses of paddy rice expansion. Additionally, to date, studies focused on the impact of land use change on LST are mostly based on coarse land cover maps (e.g., 1-km resolution), while crop maps with more detailed information (e.g., 10-m spatial resolution) are necessary for a better understanding of the LST driving mechanism (Du et al., 2019;(Yu et al., 2020c)). Furthermore, the influence of land use change on daily temperature could vary in daytime and nighttime. Peng et al. (2014) showed the divergent effects of daytime and nighttime LST on afforestation in China. However, the diurnal and seasonal characteristics of the impacts of paddy rice expansion on LST are seldom considered, hampering our understanding of the effects of emerging rapid rice expansion on the land surface energy budget and local climate in China's new rice bowl.

The objective of this study is to provide observational evidence from satellite remote sensing on the effects of the rapid paddy rice expansion on LST and explore the driving mechanism. We examined the effects of paddy rice expansion on LST based on satellite observations and a high-

resolution (10-m) crop map derived from Sentinel-2 imagery (You and Dong, 2020; You et al., 2021), by using a pair-wise comparison in northeast China. Results were analyzed at both diurnal and seasonal scales. Energy redistribution factor (f), an indicator of land surface energy flow via latent and sensible heat transfer (Bright et al., 2017), and albedo were subsequently examined for explanation of temperature change mechanism, based on the climatic reanalysis and remote sensing datasets.

2. Materials and methods

2.1. Study area

Northeast China is a cold-humid region that extends from 38.713° N to 53.546° N in latitude and from 121.146° E to 123.620° E in longitude. The region is composed of Heilongjiang, Jilin, Liaoning Provinces, and the east part of the Inner Mongolia Autonomous Region. The climatic conditions here are temperate humid or sub-humid continental monsoon climate (Liu et al., 2018). Since the 1950s, the rapid land use transition, with farmlands expanding, made cultivated land the dominant land use type of the region (Yan et al., 2018). In Heilongjiang province, for example, the increased rice area from 1951 to 2018 accounted for 8.44% of the province's total area (Hu et al., 2021). In particular, paddy fields increased 1.78 times from 1982 to 2015 in Sanjiang Plain which is the main paddy rice base in Heilongjiang Province. Within the last two decades, upland crop planting in the study area has been strikingly reclaimed into paddy rice planting with an average annual increase rate of 2.0×10^5 ha per year (Xin et al., 2020) due to higher profitability and elevated hydrothermal conditions, especially in Sanjiang Plain where the paddy fields increased by 60% from 2000 (4.77 \times 10⁶ ha) to 2014 $(7.63 \times 10^6 \text{ ha})$ (Dong et al., 2016). Fig. 1 illustrates the location and the distribution of major crop types of the region in 2017 (You et al., 2021).

Crop growth in northeast China was separated significantly in stages, which is distinguished among different crop types (Table 1). Generally, rice paddy was flooded from early to mid stages in May, and the field surface contained substantial water from the beginning of the flooding period until the tillering period. While corn and soybean were both in the initial stage from mid May to early June, and the land surface was represented by bare soil mostly. Thus, surface biophysical characteristics altered notably along with rice expansion due to the transformation of crop phenological stages as well as the change of agricultural administration, especially between upland fields and rice paddies.

Monthly enhanced vegetation index (EVI) and land surface water index (LSWI) data highlighted the divergence of surface biophysical characters between rice paddy and upland crop fields (Xiao et al., 2005). Relative to the same trends, EVI was affected mainly by the growth condition of crop leaves. Moreover, larger LSWI was detected on rice paddy from May to June, which presented higher land surface moisture conditions than the upland crop fields.

2.2. Satellite data processing

Remote sensing data were used to investigate the differences of surface biophysical factors in three major crops (paddy rice, corn, and soybean) in northeast China. A range of surface parameters was compiled as data products, including the MODIS land surface products. The MODIS data included average 8-day 1-km daytime and nighttime LSTs (MYD11A2_V6) and daily 16-day 500-m albedo (MCD43A3_V6) model datasets (Fig. 2). The LST data were derived from Aqua/MODIS instrument imaging the entire Earth twice a day, at both daytime (local solar time \sim 1:30 PM) and nighttime (\sim 01:30 AM). Importantly, these times are close to those at which the maximum and minimum temperatures were expected during a whole day (Duveiller et al., 2018a). Each pixel value in MYD11A2_V6 represents an average of all the corresponding daily LST pixels within that 8-day period. Pixel artifacts, caused by cloud, cloud shadow, and other adverse conditions, are not

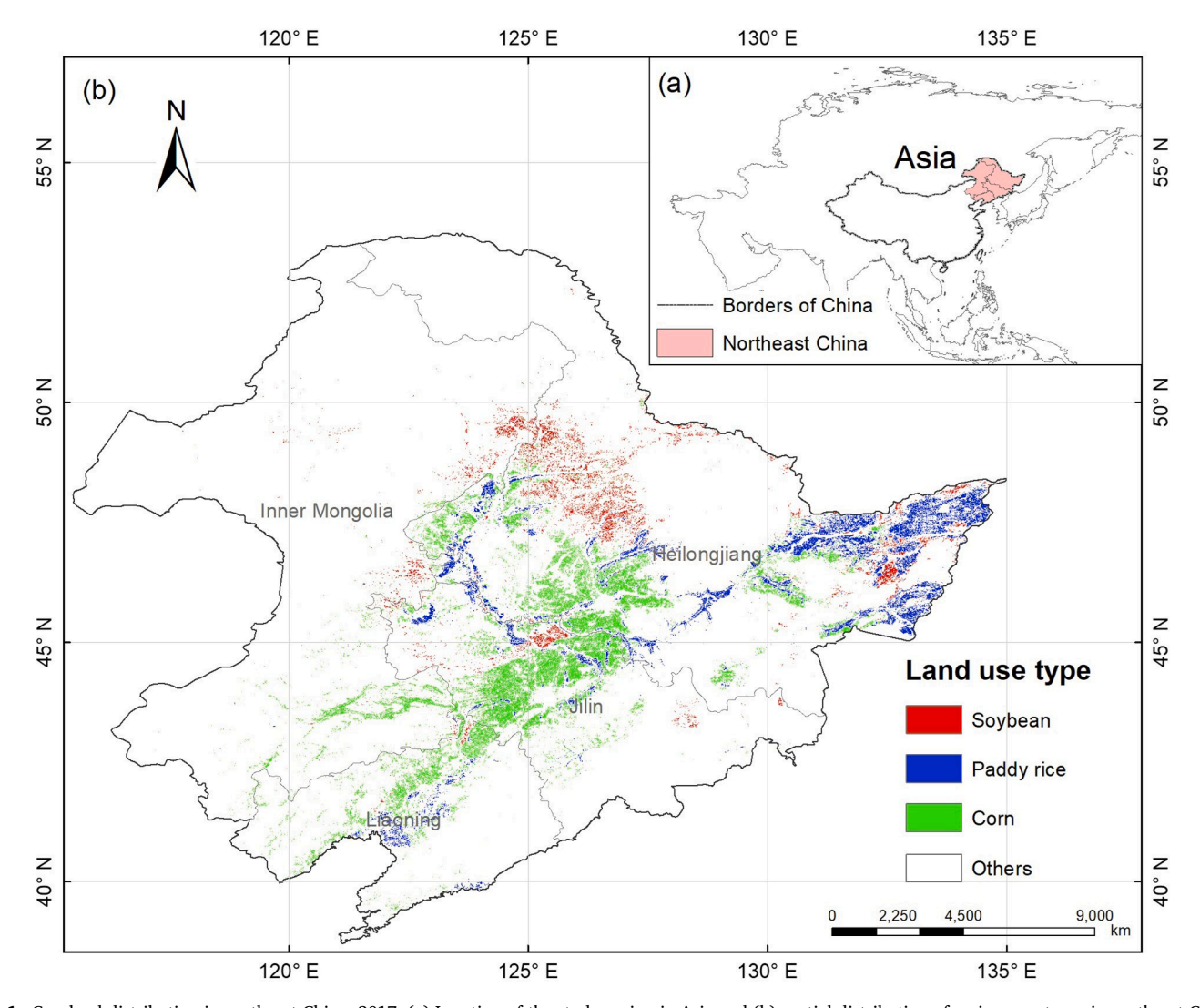


Fig. 1. Cropland distribution in northeast China, 2017. (a) Location of the study region in Asia and (b) spatial distribution of major crop types in northeast China with 1 km spatial resolution, spatially aggregated from the 10-m crop map (You et al., 2021).

Table 1
Crops' calendars from May to September. Phenological stages of three main crops are elucidated within the early (E), mid (M), and late (L) periods in a month.

Month	May			Jun			Jul			Aug			Sep		
Ten-day	E	M	L	E	M	L	E	M	L	E	M	L	E	M	L
Paddy rice	1		2	3	4				5	6		7			8
Corn		1	2	3		4		5				6		7	8
Soybean			1	2	3			4	5						6

Paddy rice: 1-Seeding/Flooding, 2-Transplanting, 3-Reviving, 4-Tillering, 5-Booting, 6-Heading, 7-Milk stage, 8-Mature and harvest. Corn: 1-Sowing, 2-Seeding/Three leaves, 3-Seven leaves, 4-Stem elongation, 5-Heading, 6-Milk, 7-Mature, 8-Harvest. Soybean: 1-Sowing, 2-Seeding, 3-The 3rd true leaf, 4-Flowering, 5-Pod setting, 6-Mature and harvest.

produced but represented as null value, which were excluded in our further analysis. Thus, we filtered all the empty values for the statistical analyses of the LSTs of different crops. The albedo data included both directional hemispherical reflectance (black sky albedo) and bihemispherical reflectance (white sky albedo) for a shortwave (0.3–5.0 μ m) broad-spectrum band (Schaaf et al., 2002). To obtain an estimate of real conditions without information on the fraction of diffuse radiation, we took the mean of both values in our data analyses (Duveiller et al., 2018b).

In addition, climate data were also derived from the Famine Early Warning Systems Network Land Data Assimilation System (FLDAS) dataset, the TerraClimate monthly reanalysis data, and a 0.5^{\prime}

downscaled dataset with bilinear interpolation for air temperatures at 2 m (Peng, 2019). The TerraClimate monthly reanalysis data was a dataset of monthly climate and climatic water balance for global terrestrial surfaces including downward surface shortwave radiation (Abatzoglou et al., 2018). The FLDAS dataset includes information on many climate-related variables including the monthly downward longwave radiation flux data, which was usually used in the temperature response model (McNally et al., 2017). The 0.5′ downscaled dataset of air temperature at 2 m was developed with bilinear interpolation and published in Network Common Data Form (at https://doi.org/10.5281/zenodo. 3185722) (Peng, 2019). Here the monthly mean air temperature was obtained to estimate the surface energy redistribution factors and to

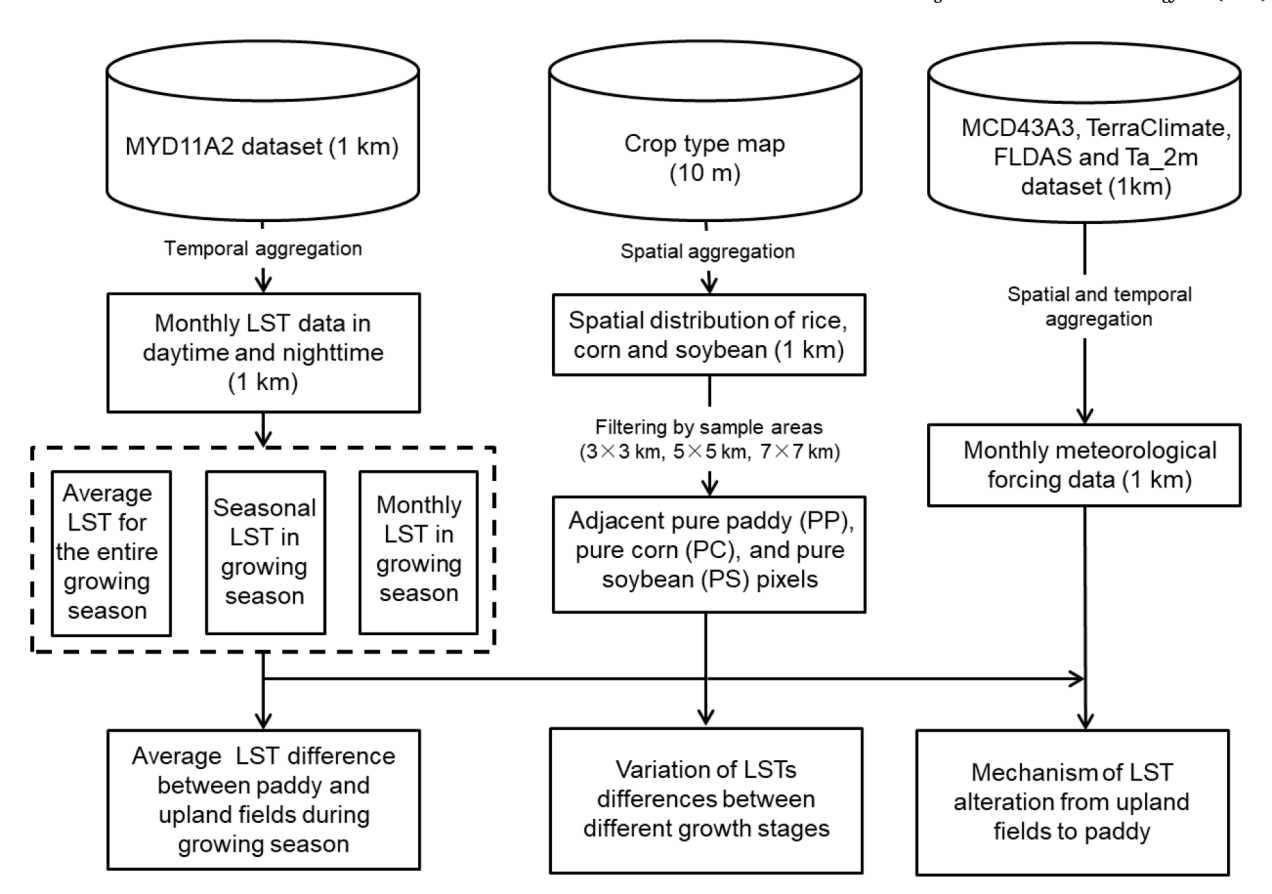


Fig. 2. The workflow of this study. Raw datasets marked in cylinders included the average 8-day 1-km daytime and nighttime land surface temperature (MYD11A2) dataset, the daily 16-day 500-m albedo (MCD43A3_V6) dataset, monthly downward longwave radiation flux (FLDAS), monthly downward longwave radiation flux (TerraClimate), and the monthly 2-m air temperature dataset. Specific operations used to derive new datasets with different spatial and temporal resolutions are indicated by descriptions on arrows. The land surface temperature (LST), albedo, and energy redistribution factor (f) of core crops in the study area were analysed following the workflow.

calculate the divided temperature responses through radiative or non-radiative processes. All the remote sensing data were resampled to 1-km spatial resolution for statistical analyses and pair-wise comparison.

Based on our previous studies, a new 10-m crop map with an overall accuracy of 91% was used (You and Dong, 2020; You et al., 2021). The crop map was generated by using available Sentinel-2 imagery, intensive ground truth data, and the random forest classifier in the Google Earth Engine. The resulting map depicts the spatially explicit information of the key crops of northeast China. This 10-m crop map was aggregated to generate three 1-km crop area proportion maps (i.e., paddy rice, corn, or soybean) to match the spatial resolution of other satellite remote sensing data. We then filtered those pixels in which the single crop type dominated (>80% coverage) the 1-km pixel. Thus, the resulting filtered pixels have a relatively high proportion of planting areas for certain crop types which here is considered pure pixels (pure paddy rice, PP; pure corn, PC; or pure soybean, PS). All the data were derived from satellite and crop maps for 2017.

2.3. Temperature response model

Based on a linearization of the surface longwave radiation term of the surface energy balance equation, Bright et al. (2017) formulated an analytical expression to estimate the direct surface temperature response to land use and cover change. The temperature response model was widely used in land surface temperature research, to isolate the contribution to the model-predicted ΔT from each biophysical factor associated with land cover conversion (Zhao et al., 2014). To obtain calculated ΔT_s value that is more closer to the observations, we used the modified temperature response model which estimated the ΔT_s by (1 +

 $f(1 + f + \Delta f)$ instead of $(1 + f)^2$ (Liu et al., 2019b):

$$\Delta T_{s} = \frac{\lambda_{0}}{(1+f)} \Delta R_{n}^{*} + \frac{-\lambda_{0}}{(1+f)} \Delta G + \frac{-\lambda_{0}}{(1+f)(1+f+\Delta f)} (R_{n}^{*} - G) \Delta f$$
 (1)

where λ_0 is the monthly mean Planck response to the external radiative forcing at the surface calculated as $1/4\varepsilon_s\delta T_s^3$ (where ε_s is the monthly mean surface emissivity approximated as a constant 0.97 based on previous empirical findings (Song et al., 2014; (Liu et al., 2019b)), T_s is the monthly mean land surface temperature); ΔG is the change in the monthly mean heat diffused into/out of the subsurface medium (G is estimated as $0.14(T_{a,n}-T_{a,n-1})$, where n is the time series of the month); f is the energy redistribution factor which can be calculated using:

$$f = \frac{\lambda_0}{T_s - T_a} (R_n - G) - 1 \tag{2}$$

where T_a is the monthly mean air temperature at 2 m; the Rn^* is the monthly mean apparent net radiation, which could be computed as:

$$R_n^* = (1 - \alpha) * S + L_{\downarrow} - \delta T_a^4 \tag{3}$$

where α is the monthly mean surface albedo; S is the monthly mean downward shortwave radiation flux, $(1-\alpha)*S$ means net shortwave radiation flux, L_{\downarrow} is the monthly mean downward longwave radiation flux, δ is the Stefen-Boltzmann constant.

Based on the crop map, the monthly mean values of f on the rice paddy and upland crop fields were calculated separately, then were used to estimate partial land surface response by radiative or nonradiative methods, corresponded with values of observed albedo and other factors

(evapotranspiration, etc.). In this analysis, we assume that R_n^* , f, and G are parameters affected by the crop types (rice, corn, or soybean) and are independent of T_s (Bright et al., 2017). Thus, the first, second, and third right-hand terms in Eq. (1) are the response to the surface radiative forcing from the albedo change ($\Delta T_s.alb$), the change in heat conducted by the surface medium ($\Delta T_s.G$), and the change in turbulent energy redistribution ($\Delta T_s.f$), respectively (Bright et al., 2017). In this study, the surface medium induced temperature variation was negligible in whole growing seasons, hence the model calculated $\Delta T_s.cal$ was presented as the sum of $\Delta T_s.alb$ and $\Delta T_s.f$.

2.4. Pair-wise comparison

To quantitatively investigate the impacts of paddy rice expansion on LST, we used a pair-wise comparison approach ((Liu et al., 2019b)) to compare PP pixels with adjacent PC or PS pixels, respectively. To exclude the effects caused by background noises like atmospheric circulation, we considered the following two factors: 1) Minimizing the influences of spatial heterogeneity caused by atmospheric background, and 2) covering enough pure pixels of contrasting crop types within the neighbourhoods (Alkama and Cescatti, 2016; Wang et al., 2018). In this study, we mainly discussed the comparison based on $5\times 5~{\rm km}$ sampling areas which worked well for the above two rules. Moreover, we also explored the climatic effects of paddy rice expansion both on a larger scale (7 \times 7 km sampling areas) and smaller scale (3 \times 3 km sampling areas) to demonstrate the robustness of the conclusion we obtained within 5 \times 5 km sampling areas.

Concretely, we divided the entire study area into 5×5 km sampling areas and selected those areas considering the two factors associated

with atmospheric circulation, with two compared crop type conversions (PP and PC, or PP and PS) and a small elevation range ($\sim \pm 100$ m). In total, we selected 212 and 63 sample areas to compare PP and PC, or PP and PS, respectively. Within each sample area, the adjacent PC and PS pixels were selected to pair with PP pixels, providing an opportunity to compare different LST indicators (daytime LST, nighttime LST, daily mean LST, and diurnal LST range (DTR)) and other biophysical proxies. Daily mean LSTs were estimated from the arithmetic mean of maximum (daytime) and minimum (nighttime) LSTs. A previous study showed that the typical physical properties of rice paddy are distinct in different months and are particularly characterized as standing water in May and June (Yu and Liu, 2019). To reflect this phenological difference, we divided the growing season into two stages: May and June (G1), and July to September (G2). Within each sample area, the daytime, nighttime, daily mean difference in LST (\Delta LSTs) and diurnal LST range (Δ DTRs), as well as differences in albedo and f (Δ albedo and Δf) between PP and PC/PS, were calculated based on the arithmetic means of each crop type respectively. Variations were then assessed at the monthly and growth stage scales throughout the entire growing season (May to September). The technical flow of the study is shown in Fig. 2.

3. Results

3.1. Comparisons of LST between paddy rice and upland field crops throughout the entire growing season

To quantitatively characterize the impacts of paddy rice expansion from upland field crops, we performed a pair-wise comparison between PP and PC/PS, respectively, for different temperature indicators within

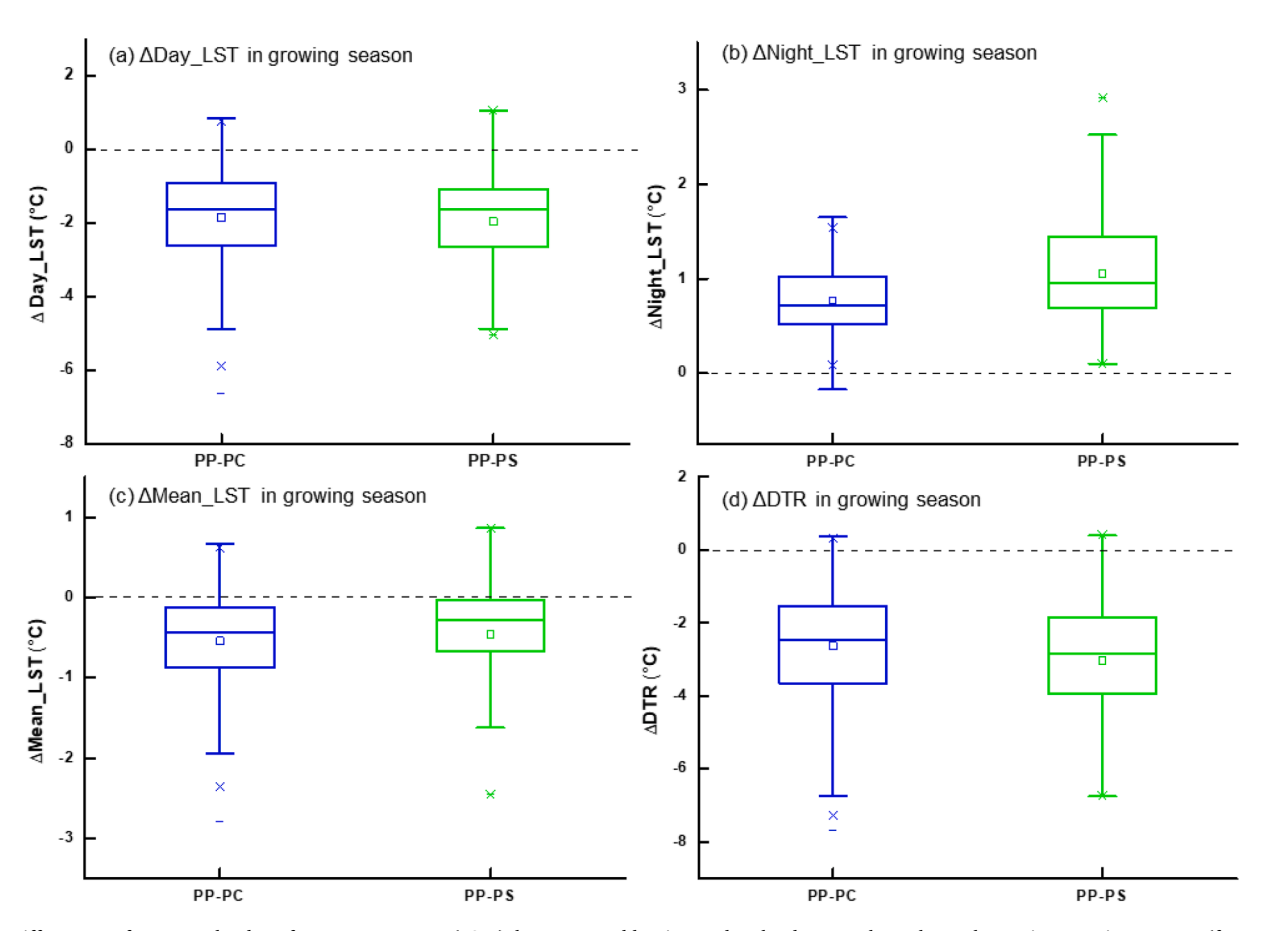


Fig. 3. Differences of average land surface temperatures (LSTs) between paddy rice and upland crops throughout the entire growing season (from May to September). The differences of (a) daytime, (b) nighttime, and (c) daily mean LST as well as (d) diurnal temperature range (DTR) between pure paddy rice pixels (PP) and the adjacent pure corn pixels (PC) and pure soybean pixels (PS) in northeast China. The middle lines and the rectangles within boxes represent the median and average values of ΔLSTs, respectively.

each filtered sample area throughout the whole growing season (from May to September), including daytime LST, nighttime LST, daily mean LST, and DTR (Fig. 3).

The PP showed lower daytime LST by $-1.8\pm1.3~^{\circ}C$ and higher nighttime LST by 0.8 \pm 0.4 $^{\circ}C$ compared with PC (Fig. 3a and b), which demonstrated that the conversion from PC to PP decreased daytime LST and increased nighttime LST. Similarly, but to a greater extent, the transition of PP from PS caused more dramatic changes in both daytime (lower LST of PP than PS by $-2.0\pm1.3~^{\circ}C$) and nighttime LST (higher LST of PP than PS by $1.1\pm0.5~^{\circ}C$) than that from PC.

Comparing to the daytime cooling caused by conversion from PC/PS to PP, the magnitude of nighttime warming was smaller, with a reduction in daily mean LST by $-0.5\pm0.6~^{\circ}\text{C}$ and $-0.5\pm0.7~^{\circ}\text{C}$, respectively (Fig. 3c). In addition, the small range of DTR for PP was observed in both comparisons for PC ($-2.6\pm1.5~^{\circ}\text{C}$) and PS ($-3.0\pm1.5~^{\circ}\text{C}$) (Fig. 3d). These results indicated that throughout the entire growing season, the LST of PP was lower in the daytime and higher at nighttime than that of adjacent PC and PS, contributing to lower daily mean LST and smaller DTR

At the monthly scale, we found that the average daytime $\Delta LSTs$ between PP and PC/PS were negative for all months, while nighttime $\Delta LSTs$ showed opposite warming effects during the whole growing season (Fig. 4a–d). The asymmetric monthly cycle of variation for LST, caused by conversion from upland crops to paddy rice, was found both in the daytime and nighttime. The differences of the daytime ΔLST

between PP and PC demonstrated a maximum cooling effect in May by -3.7 ± 2.4 °C, while the maximum nighttime Δ LST (1.7 \pm 0.6 °C) occurred in June. Overall, daily mean ΔLST between PP and PC were negative in all months with a maximum difference in May (-1.3 ± 1.1 °C) which due to the effects of lower LST in daytime offset the effects of higher LST in nighttime (Fig. 4a-c). Similar results were found between PP and PS with a magnitude of $-3.8 \pm 2.4\,^{\circ}\text{C}$ in daytime Δ LST and $2.0 \pm$ 0.9 °C in nighttime Δ LST, which subsequently led to a slightly smaller decrease in daily mean ΔLST ($-1.1\pm1.4~^{\circ}C)$ in May than that between PP and PC. Furthermore, Fig. 4d showed that the Δ DTR reached the highest values in early months, which was found in May between PP and PS (-5.3 \pm 2.6 °C) and in June between PP and PC (-5.9 \pm 2.5 °C). These findings highlighted the stronger effect of paddy rice expansion during the early season. Similar results were obtained from the calculations based on smaller and larger sample areas. In 3 imes 3 km sample areas, the daily mean LST of paddy is cooler than corn or soybean field by $-0.3\pm0.2~^{\circ}\text{C}$ (SI Appendix, Fig. S1) during the entire growing season. Results calculated within 7 \times 7 km sample areas showed a $-0.5~\pm$ 0.4 °C difference of daily mean LST between PP and PC, or PS in the entire growing season (SI Appendix, Fig. S2).

3.2. Pair-wise comparison between rice paddy and upland field crops in the different growth stages

The previous results showed that the maximum magnitude of both

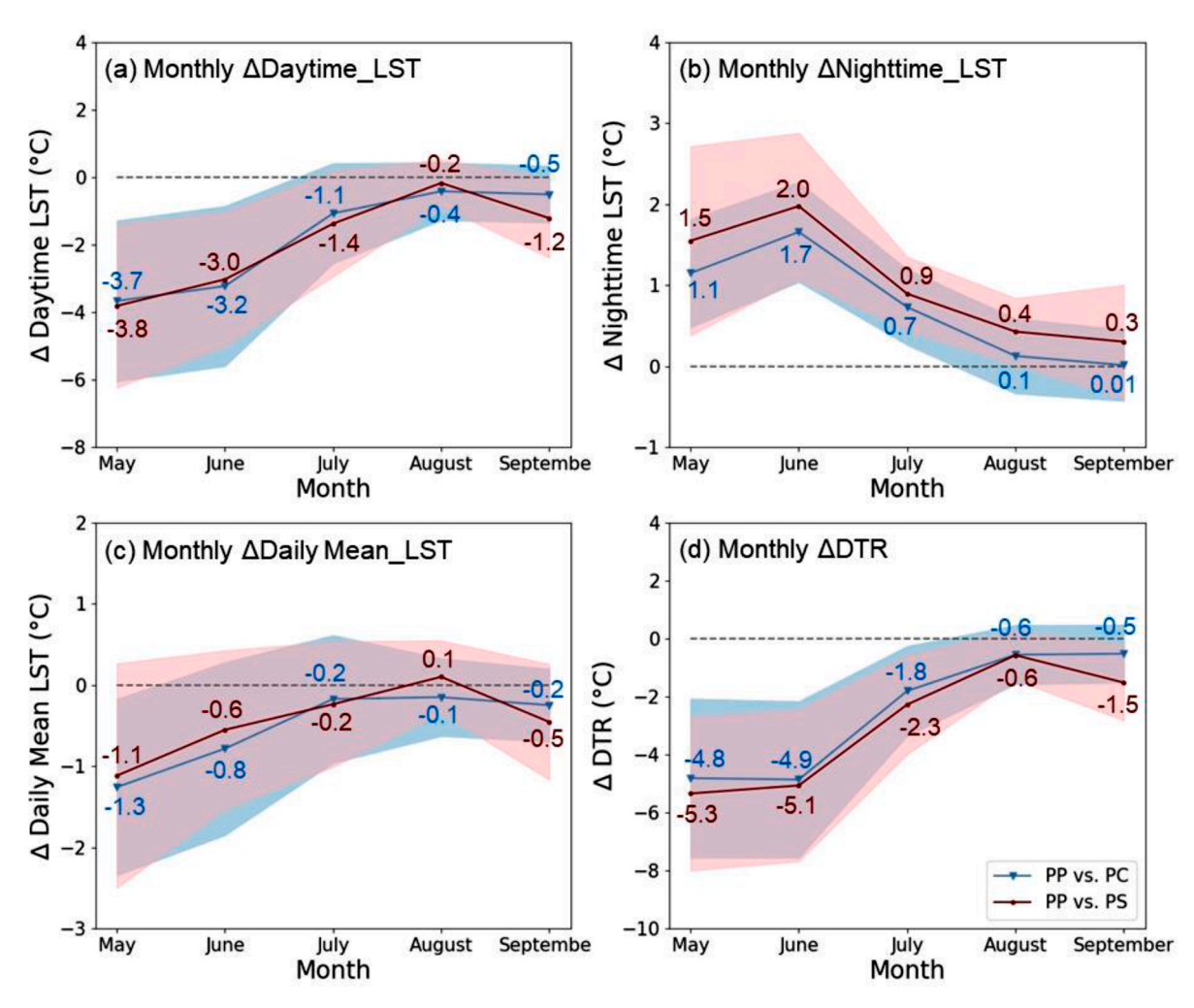


Fig. 4. Differences of monthly average land surface temperatures (LSTs) between paddy rice and upland crops. Differences in the monthly average (a) daytime, (b) nighttime, (c) daily mean LSTs, and (d) diurnal LST range (DTR) between pure paddy rice pixels (PP) and the adjacent pure corn pixels (PC) and pure soybean pixels (PS) in northeast China. Shaded areas represent the standard deviation (SD) of all samples.

daytime cooling and nighttime warming was detected in the early season, namely May and June. To better understand the changes of LST caused by surface biophysical characteristics driven by crop phenology, we analyzed the average Δ LSTs between the rice paddy and upland field crops in the early growth stage (G1; i.e., May and June) and the late growth stage (G2; i.e., July to September), separately (Fig. 5).

Daytime LST of PP was lowered by 3.4 \pm 2.2 °C than PC, and 3.4 \pm 2.1 °C than PS in G1, while differences in G2 were -0.7 ± 0.9 °C and -0.9 ± 0.9 °C, respectively (Fig. 5a). In contrast, nighttime ΔLST was 1.4 \pm 0.6 °C between PP and PC, and was 1.7 \pm 0.9 °C between PP and PS in G1, with notably larger differences in G2 (0.3 \pm 0.4 $^{\circ}\text{C}$ and 0.6 \pm 0.4 °C), respectively (Fig. 5b). Daytime cooling together with nighttime warming that are demonstrated by the Δ LST ultimately led to a decrease in the diurnal variation of LST (Δ DTR) (Fig. 5d). The magnitude of Δ DTR reduction was substantially larger in G1 (-4.8 ± 2.6 °C and -5.2 \pm 2.4 °C) than in G2 (-1.0 ± 1.0 °C and 1.4 \pm 1.0 °C). The average daily mean Δ LST was negative in both G1 and G2, with a larger reduction in G1 than in G2 between PP and PC (-1.0 ± 1.0 °C and -0.2 ± 0.5 °C) (Fig. 5c). A similar variation of daily mean ΔLST was found between PP and PS in both G1 (-0.9 ± 1.1 °C) and G2 (-0.2 ± 0.4 °C). It is noteworthy that both paddy rice transitions from corn and soybean had remarkably more prominent impacts on LST in G1 (May and June) than in G2 (July to September). Further inspection of evapotranspiration and albedo with paddy rice expansion might provide plausible explanations for the daytime and nighttime LST changes.

3.3. Biophysical mechanism of LST variation

To further understand the underlying mechanism of LST variation caused by the conversion from upland field crops to paddy rice, we calculated the energy redistribution factor (f) and the estimated Δ LSTs based on the temperature response model (Eq. (1)) driven with gridded observations observed by remote sensing approaches.

Pair-wise comparison of albedo and f between PP and the adjacent PC (Fig. 6a-b) or PS (Fig. 6c-d) illustrated that conversion from upland field crops to paddy rice led to change in geophysical forcings of surface energy. The albedo is typically higher in the upland field compared to paddy in most of the growing season. Specifically, the ΔAlbedo between PP and PC were negative from May to July (Fig. 6a), with the maximum magnitude of difference represented in June (-0.044 ± 0.022). Results were opposite in August and September with positive ΔAlbedo. The period with negative ΔAlbedo between PP and PS was longer (from May to August) than that between PP and PC during the growing season, with the largest difference of -0.033 ± 0.023 in June (Fig. 6c). Generally, higher values of f imply a greater efficiency to dissipate energy from the surface by its intrinsic biophysical properties. Monthly heterogeneity of f was detected in all three crops that showed in Fig. 6b and Fig.6d. Throughout the growing season, the mean value elevated initially (May and June) and then decreased rapidly in the late season (August and September) with a maximum value in July. Collectively, a markedly higher value of monthly mean f on paddy than upland field was detected during the entire growing season, although the seasonal patterns are similar.

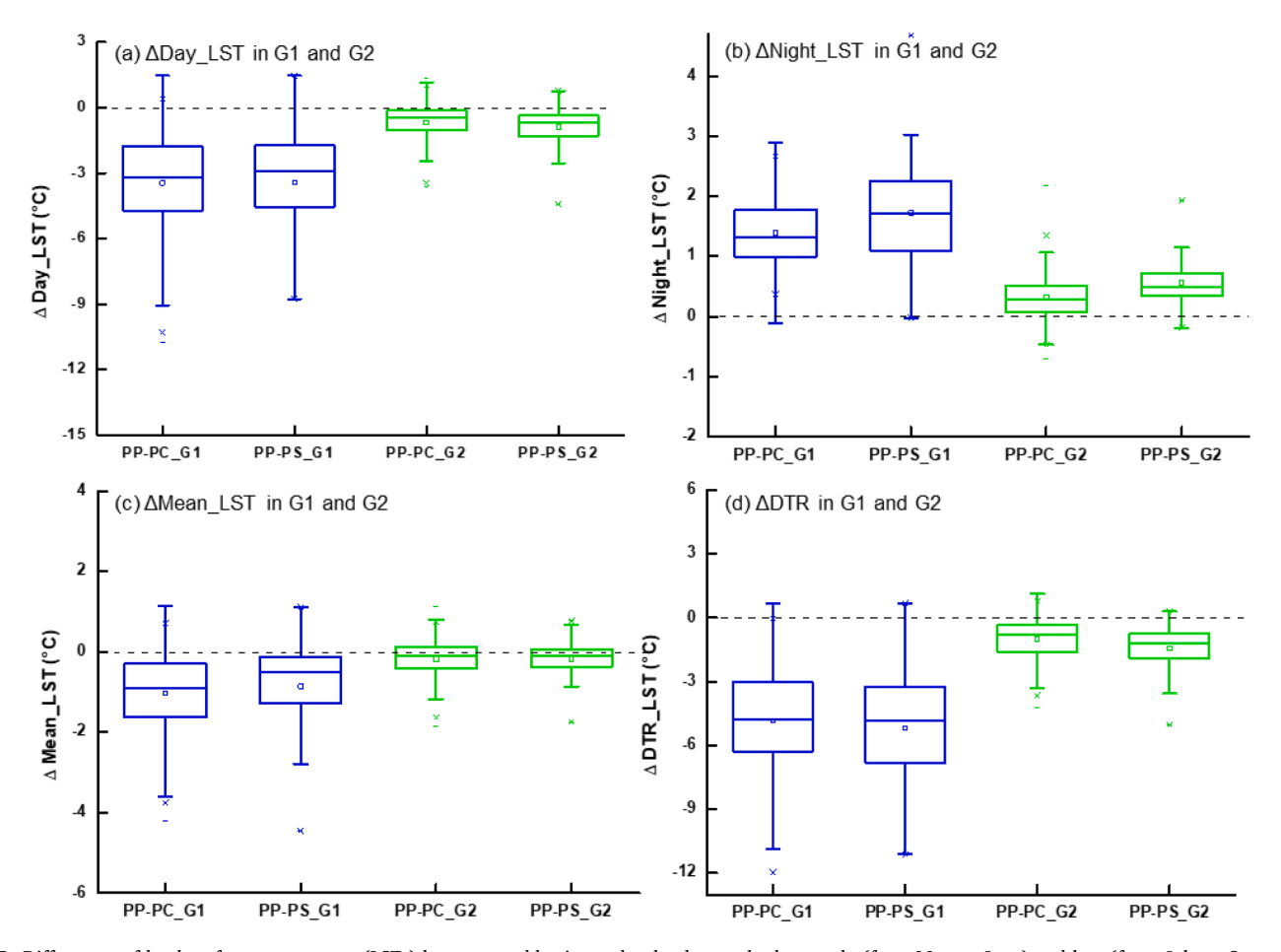


Fig. 5. Differences of land surface temperature (LSTs) between paddy rice and upland crops both at early (from May to June) and late (from July to September) growth stages. Differences in the (a) daytime, (b) nighttime, (c) daily mean LSTs, and (d) diurnal LST range (DTR) between pure paddy rice pixels (PP) and the adjacent pure corn pixels (PC) and pure soybean pixels (PS) in early growth stage G1 (May and June) and late growth stage G2 (July to September). The middle lines and the rectangles within boxes represent the median and average values of ΔLSTs, respectively.

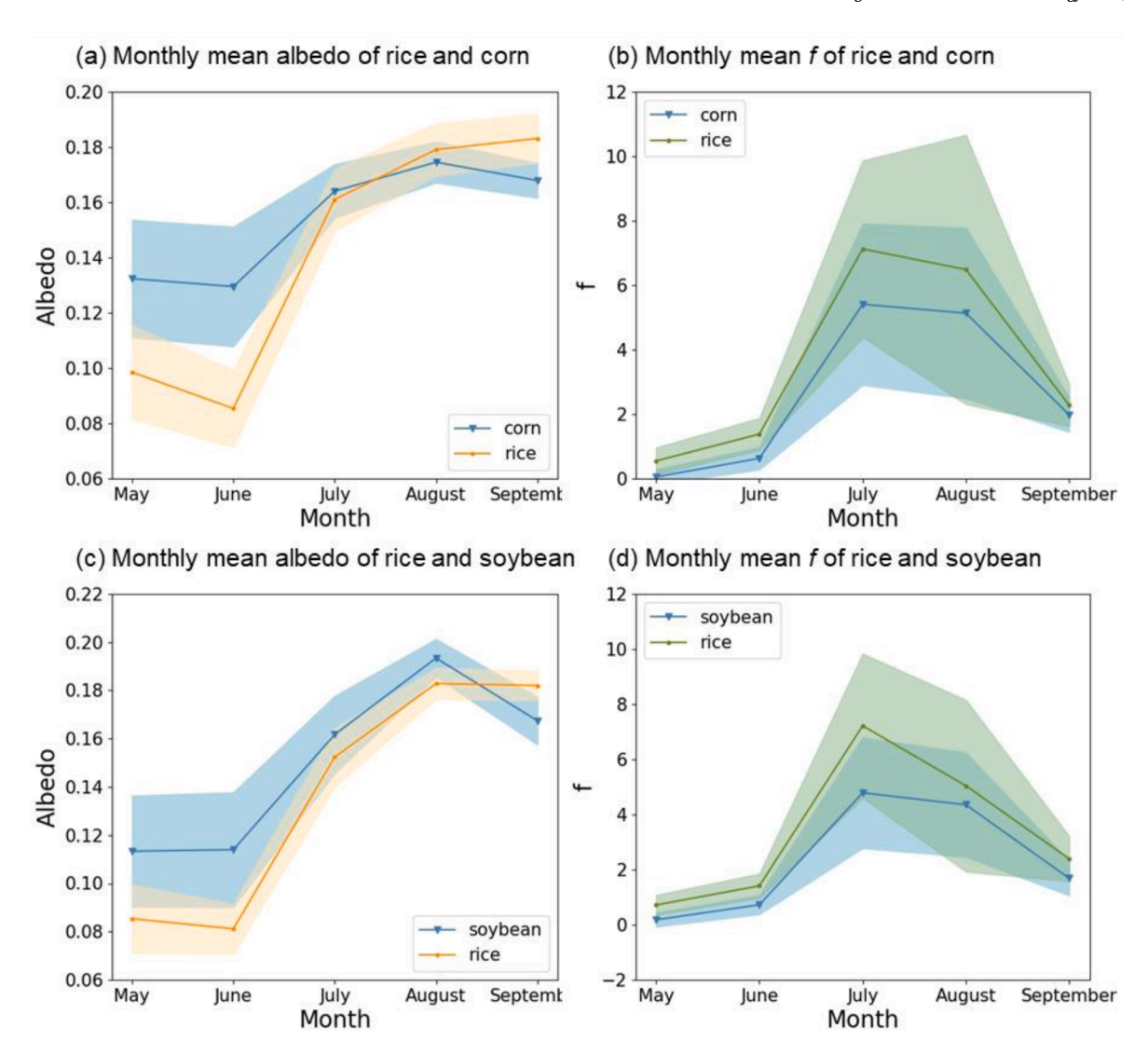


Fig. 6. Monthly mean albedo and energy redistribution factor (f). The monthly mean value of albedo (a and c) and f (b and d) for rice, corn, and soybean within adjacent sample areas. Lightly shaded areas in panels represent the standard deviation (SD) of all samples.

As incoming solar radiation was assumed to be similar between adjacent PP and PC or PS pixels, larger albedo implied stronger reflectance of radiation from the surface and more energy dissipation that may control the incoming energy in the surface energy balance. Conversely, the higher values of f may correspond to greater efficiency by the vegetated ecosystem to dissipate energy from the surface due to its intrinsic biophysical properties (Bright et al., 2017). The partition of the response by ΔT_s into contributions from changes to individual mechanisms (temperature change induced by albedo and energy redistribution factor) was calculated based on the temperature response model, as well as the comparison between the calculated ΔT_s (ΔT_s cal) and the ΔT_s derived from remote sensing data (ΔT_s r) (Fig. 7).

In most of the months during the growing season, cooling effects dominate the LST response by comparison between rice and upland crops, owing to a negative Δf signal outweighing a positive Δalbedo signal. The difference between albedo induced ΔT_s ($\Delta T_s.alb$) and f induced ΔT_s ($\Delta T_s.f)$ were acute especially in the early growth period (G1). In May, for instance, lower albedo on paddy rice warming the surface at about 1.44 °C and 1.08 °C compared with corn (Fig. 7a) and soybean (Fig. 7c) separately. While the effects of nonradiative processes, including evapotranspiration and turbulent heat exchange, can lead to a -5.01 °C and -4.98 °C cooling compared to corn and soybean, respectively. In total, $\Delta T_s.cal$ was negative from May to September illustrating

the cooling effect of rice compared to both corn and soybean, especially in G1 (May and June). Fig. 7b and Fig.7 d) showed that the model calculated ΔT_s was consistent with the ΔT_s derived from remote sensing data (MODIS data). RSME and R^2 of these two estimated ΔT_s between PP and PC (RMSE=0.11, R^2 =0.993), or PS (RMSE=0.09, R^2 =0.996) were calculated in parallell, indicating that the two elements (ΔT_s alb and ΔT_s f) of the temperature responses can better reflect the radiative and nonradiative process in regulating LST. Consistency of two estimated ΔT_s between PP and PC, or PS maintained both on a larger and smaller scale (SI Appendix, Figs. S3 and S4).

4. Discussion

4.1. The driving mechanism of regional LST change

Surface albedo and energy redistribution factor (f) are crucial factors in land surface biophysical process research (Zhou et al., 2016; Abera et al., 2020; Zhou et al., 2020). Generally, the decrease of albedo results in extra energy absorption and warms the land surface, which is manifested by an increase of LST. On the contrary, an increase of f means more energy dissipation through moisture exchange, which triggers a cooling effect. Temperature response model synthesizes biophysical factors and divided the Δ LST into separate ingredients namely radiative

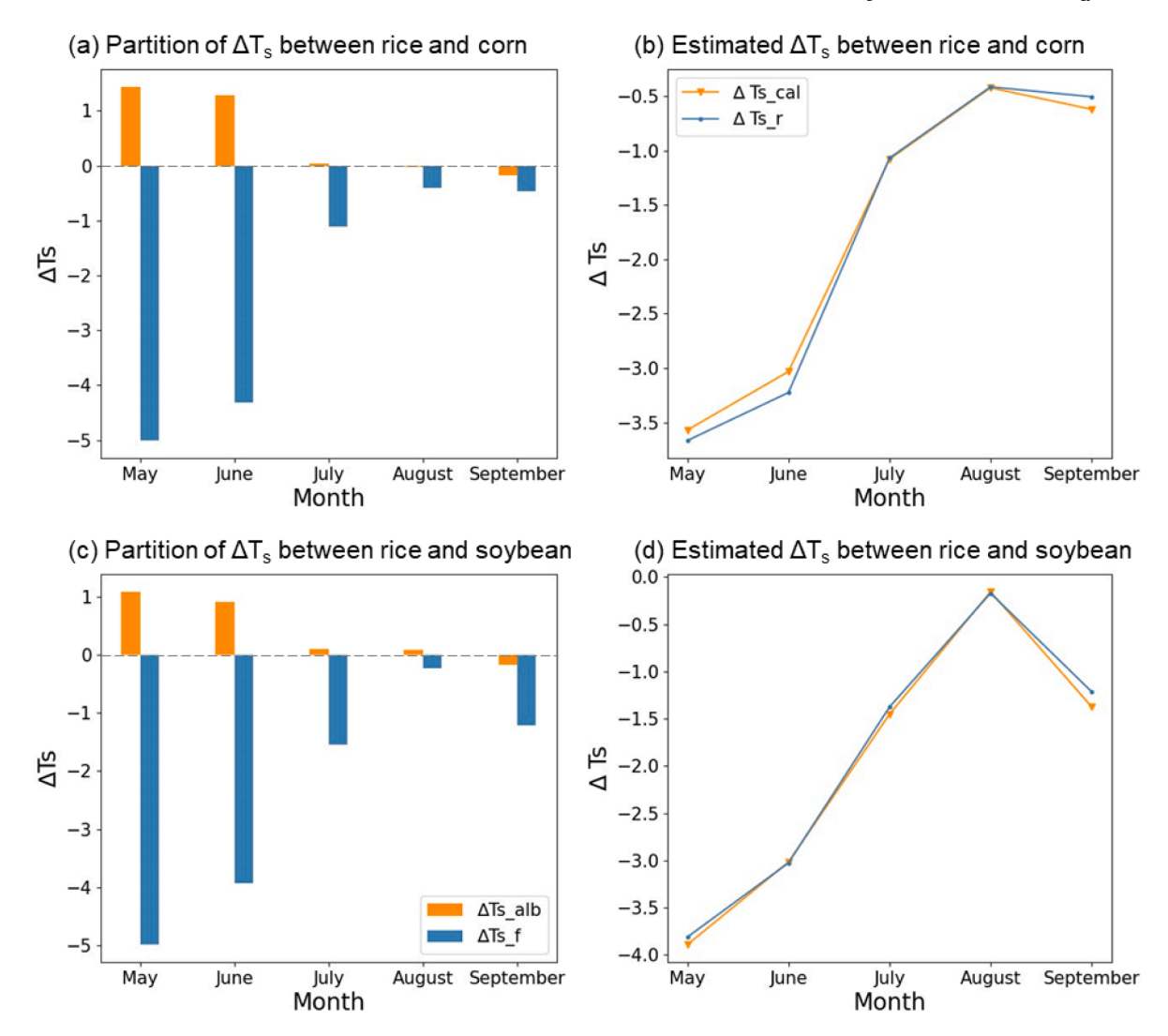


Fig. 7. ΔT_s partition based on temperature response model and correlation with ΔT_s derived from MODIS data. The ΔT_s (difference of land surface temperature) estimated based on the energy balance model ($\Delta T_s.cal$), and contribution from albedo change ($\Delta T_s.cal$) and energy redistribution factor change ($\Delta T_s.f$), compared between pure paddy rice pixels (PP) and pure corn pixels (PC) (a), and pure soybean pixels (PS) (c). Correlations between ΔT_s derived from remote sensing data ($\Delta T_s.f$) and $\Delta T_s.cal$ based on LST comparison between PP and PC (b), and PS (d).

 Δ LST (induced by albedo alteration) and nonradiative Δ LST (induced by energy redistribution change), which is beneficial to understanding temperature change mechanisms via land cover transition. As demonstrated, we found the biophysical energy changes accompanying farmland transformations, namely cooling down of nonradiative process or heating up of the radiative process, and the combination of these two ingredients contributed to a net cooling effect of average daily LST in G1. These results are consistent with previous studies that examined the climate effects of marshland loss (Shen et al., 2020), irrigation (Krishnankutty Ambika and Mishra, 2019), and paddy rice expansion that is based on multi-year data (Pan et al., 2020).

However, the response model of climatic feedback could be more complex and compounded by multiple factors. Furthermore, the effects of albedo and f on LST are local and may vary with latitude (Prevedello et al., 2019). Attribution analyses of biophysical process feedback of land use conversions to climate have demonstrated that pathways of effects are multiple and might go beyond simple albedo or f change (Schwaab et al., 2020; (Yu et al., 2020b); Zhang et al., 2020; Zheng et al., 2020). The Δ LST caused by the change of f demonstrated the comprehensive effects of aerodynamic resistance, the Bowen ratio (that affected by both sensible heat flux and latent heat flux), total heat transfer resistance, and so on (Wang et al., 2020). Indeed, the more specific

distributions to each factor, such as the distributions between sensible heat flux and latent heat flux are not evaluated. Aerodynamic resistance, for instance, is found to play an important role in regulating energy flows between the land surface and the atmosphere (Zhao et al., 2015; Moon et al., 2020), attributed to the alteration of sensible heat flux caused by aerodynamic roughness change (Lee et al., 2011). It is also demonstrated as the dominant factor of biophysical impacts on climate in the Earth greening process (Chen et al., 2020). The regional climatic condition could also alter the biophysical processes, which make the surface biophysical processes more regional relative to the biogeochemical processes (Zhao and Jackson, 2016; Zhao et al., 2019). Furthermore, the LST alone is not sufficient for understanding near-surface energy transformation and atmospheric circulation, which is essential to understand air temperature (Ikawa et al., 2021) and should be explored deeper in the future. As a preliminary analysis by variation of albedo and f, here, we merely supported a coarse biophysical mechanism explanation of LST change based on large scale remote sensing data, while a comprehensive analysis of multi-factor influence mechanisms is indispensable in further studies.

4.2. The divergence of time scale in surface biophysical processes study

Previous assessments of climatic effects on land use and land cover change are diverse depending on different time scales ranging from daily to decades (Alkama and Cescatti, 2016; Zeng et al., 2017; Duveiller et al., 2020; Lan et al., 2020; Yu et al., 2020a). These studies have already conveyed an overall finding that the magnitude of variation demonstrated seasonally asymmetric characteristics of biophysical factors. Results from equidistant time scale (e.g., monthly) studies often have competing and diverging conclusions. Simply studying longer periods may lead to a non-significant result of variation, while analyses on a fine-scale may suffer from random error (Liao et al., 2018; Abera et al., 2020). Thus, studies merely based on an equidistant time scale have little implication for the application of biophysical effects in climate models.

Past research focused on how irrigation affects climate suggests that irrigation enhances local warming with greater nocturnal warming effects than daytime cooling effects (Chen and Jeong, 2018). This result demonstrated the unsynchronized diurnal temperature response to the irrigation, which emphasized the necessity of diurnal dynamaic analyses. What's more, the biophysical process changes are directly determined by the physical characteristics of the surface to a large extent, especially on farmland which is modulated by crop phenology and agricultural management (Houspanossian et al., 2017; Duveiller et al., 2018a;(Liu et al., 2019c)). Changes in these surface physical characteristics are heterogeneous over the growing season. Rice paddy, for instance, has prominent differences amongst surface characteristics between the first two months (G1; May and June) and the later months (G2; July to September) of the growing season due to the phenology of rice growth and agricultural practices (water flooding and soaking in early-stage).

Comparing to previous studies (Du et al., 2019; Pan et al., 2020), we covered deeper analyses on unsynchronized diurnal LST effects of paddy rice expansion, as well as devided study periods based on the two growth stages (G1 and G2) of unequal length, which considering not only the significant variation of surface biophysical proxies over time, but also the mechanism explanation by surface physical characteristic changes. Thus, to obtain results that are more accurate and provide practical significance on the biophysical effect of land use change on climate, it is necessary to consider the time scale that is influenced by surface biophysical characteristic variation more than isometric time division (Duveiller et al., 2018b; Chen et al., 2020; Duveiller et al., 2020). The method is also of relevant significance in climate model studies that consider the process of land use change.

Moreover, the pair-wise comparison in this study revealed the intrinsic characteristic differences between paddy rice and the upland crop using one year of data (2017), which infers what will happen to LST if other upland crops transition to paddy rice cultivation. The high-resolution crop map allows more accurate pure pixel selection in this study, but cannot support the long-time series analyses for now due to limited crop maps at this spatial scale. A direct temporal trend of LST in the rice expansion areas would also be essential in the future when the multiple temporal crop maps are available.

5. Conclusion

This study provided evidence of the cooling impacts of paddy rice expansion and its seasonal variations at a local scale by using a space-for-time substitution method. The daily mean LST of rice paddy during the growing season (May to September) was lower when compared to that of corn and soybean fields, as a result of daytime cooling and nighttime warming, which subsequently led to a narrower diurnal LST range. Furthermore, the cooling effects were more prominent in the early growth stage (G1; May and June) than the late growth stage (G2; July to September). The lower albedo and higher energy redistribution factors were observed on paddy rice in the early season compared to the

upland crops. Normally, the higher values of f typically imply a greater efficiency to dissipate energy from the surface, while lower albedo means more net radiative energy absorption. Thus, the detected cooling effects were attributed to the domination of surface temperature response of nonradiative mechanisms aided by the radiatively induced temperature responses. Similar results were found both using larger (7 \times 7 km sampling areas) and smaller (3 \times 3 km sampling areas) sampling area scales (SI Appendix, Figs. S1-S4), which demonstrated the robustness of conclusions. This study indicates the cooling effects of paddy rice expansion and its seasonal variation, which could provide a reference for climate change researchers in paddy expansion areas in northeastern Asia and contribute to model biophysical effects of land use changes. However, the underlying climatic feedback mechanism with more systematic and in-depth quantification of their effects is still imperative. In addition, the implications of a larger scale and the remote impacts of such biophysical changes through near-surface energy transfer and atmospheric circulation should be considered in future studies.

Supporting information

Supplementary materials

Supplementary material associated with this article can be found in the attached supplementary materials file.

Declaration of Competing Interest

The authors declare that they have no known competing financial interests or personal relationships that could have appeared to influence the work reported in this paper.

Acknowledgments

This study was supported by the National Natural Science Foundation of China (No. 41871349, 41571167), the Strategic Priority Research Program (XDA19040301), the Key Research Program of Frontier Sciences (QYZDB-SSW-DQC005) of the Chinese Academy of Sciences, the U.S. National Science Foundation under Grant No. OIA-1946093, and the U.S. Geological Survey under Grant/Cooperative Agreement No. G18AP00077. This research was also a contribution from the Long-Term Agroecosystem Research (LTAR) network. LTAR is supported by the United States Department of Agriculture, which is an equal opportunity provider and employer.

Supplementary materials

Supplementary material associated with this article can be found, in the online version, at doi:10.1016/j.agrformet.2022.108820.

References

- Abatzoglou, J.T., Dobrowski, S.Z., Parks, S.A., Hegewisch, K.C., 2018. TerraClimate, a high-resolution global dataset of monthly climate and climatic water balance from 1958 to 2015. Sci. Data 5 (1), 170191.
- Abera, T.A., Heiskanen, J., Pellikka, P.K.E., Adhikari, H., Maeda, E.E., 2020. Climatic impacts of bushland to cropland conversion in Eastern Africa. Sci. Total Environ. 717, 137255.
- Alkama, R., Cescatti, A.J.e., 2016. Biophysical climate impacts of recent changes in global forest cover. Science 351 (6273), 600–604.
- Bright, R.M., Davin, E., O'Halloran, T., Pongratz, J., Zhao, K., Cescatti, A., 2017. Local temperature response to land cover and management change driven by non-radiative processes. Nat. Clim. Change 7 (4), 296–302.
- Cao, Q., Wu, J., Yu, D., Wang, W., 2019. The biophysical effects of the vegetation restoration program on regional climate metrics in the Loess Plateau, China. Agric. For. Meteorol. 268, 169–180.
- Chen, C., Li, D., Li, Y., Piao, S., Wang, X., Huang, M., Gentine, P., Nemani, R.R., Myneni, R.B., 2020. Biophysical impacts of Earth greening largely controlled by aerodynamic resistance. Sci. Adv. 6 (47), eabb1981.
- Chen, X., Jeong, S.-J., 2018. Irrigation enhances local warming with greater nocturnal warming effects than daytime cooling effects. Environ. Res. Lett. 13 (2), 024005.

- Dong, J., Xiao, X., Kou, W., Qin, Y., Zhang, G., Li, L., Jin, C., Zhou, Y., Wang, J., Biradar, C., Liu, J., Moore, B., 2015. Tracking the dynamics of paddy rice planting area in 1986–2010 through time series Landsat images and phenology-based algorithms. Remote Sens. Environ. 160, 99–113.
- Dong, J., Xiao, X., Zhang, G., Menarguez, M.A., Choi, C.Y., Qin, Y., Luo, P., Zhang, Y., Moore, B., 2016. Northward expansion of paddy rice in northeastern Asia during 2000–2014. Geophys. Res. Lett. 43 (8), 3754–3761.
- Du, G., Liu, W., Pan, T., Yang, H., Wang, Q., 2019. Cooling effect of paddy on land surface temperature in cold china based on MODIS Data: a case study in Northern Sanjiang Plain. Sustainability 11 (20), 5672.
- Duveiller, G., Caporaso, L., Abad-Viñas, R., Perugini, L., Grassi, G., Arneth, A., Cescatti, A., 2020. Local biophysical effects of land use and land cover change: towards an assessment tool for policy makers. Land Use Policy 91, 104382.
- Duveiller, G., Hooker, J., Cescatti, A., 2018a. A dataset mapping the potential biophysical effects of vegetation cover change. Sci. Data 5 (1), 180014.
- Duveiller, G., Hooker, J., Cescatti, A., 2018b. The mark of vegetation change on Earth's surface energy balance. Nat. Commun. 9 (1), 679.
- Elias, F., Ferreira, J., Lennox, G.D., Berenguer, E., Ferreira, S., Schwartz, G., Melo, L.d.O., Reis Júnior, D.N., Nascimento, R.O., Ferreira, F.N., Espirito-Santo, F., Smith, C.C., Barlow, J., 2020. Assessing the growth and climate sensitivity of secondary forests in highly deforested Amazonian landscapes. Ecology 101 (3), e02954.
- Fu, J., Jian, Y., Wu, Y., Chen, D., Zhao, X., Ma, Y., Niu, S., Wang, Y., Zhang, F., Xu, C., Wang, S., Zhai, L., Zhou, F., 2020. Nationwide estimates of nitrogen and phosphorus losses via runoff from rice paddies using data-constrained model simulations. J. Clean. Prod. 279, 123642.
- Hemes, K.S., Chamberlain, S.D., Eichelmann, E., Knox, S.H., Baldocchi, D.D., 2018.
 A biogeochemical compromise: the high methane cost of sequestering carbon in restored wetlands. Geophys. Res. Lett. 45 (12), 6081–6091.
- Houspanossian, J., Giménez, R., Jobbágy, E., Nosetto, M., 2017. Surface albedo raise in the South American Chaco: combined effects of deforestation and agricultural changes. Agric. For. Meteorol. 232, 118–127.
- Hu, X., Chen, M., Liu, D., Li, D., Jin, L., Liu, S., Cui, Y., Dong, B., Khan, S., Luo, Y., 2021. Reference evapotranspiration change in Heilongjiang Province, China from 1951 to 2018: the role of climate change and rice area expansion. Agric. Water Manage. 253, 106912.
- Huang, B., Hu, X., Fuglstad, G.-A., Zhou, X., Zhao, W., Cherubini, F., 2020. Predominant regional biophysical cooling from recent land cover changes in Europe. Nat. Commun. 11 (1), 1066.
- Huang, L., Zhai, J., Liu, J., Sun, C., 2018a. The moderating or amplifying biophysical effects of afforestation on CO2-induced cooling depend on the local background climate regimes in China. Agric. For. Meteorol. 260-261, 193–203.
- Huang, L., Zhai, J., Sun, C.Y., Liu, J.Y., Ning, J., Zhao, G.S., 2018b. Biogeophysical forcing of land-use changes on local temperatures across different climate regimes in China. J. Clim. 31 (17), 7053–7068.
- Hwang, Y., Ryu, Y., Huang, Y., Kim, J., Iwata, H., Kang, M., 2020. Comprehensive assessments of carbon dynamics in an intermittently-irrigated rice paddy. Agric. For. Meteorol. 285-286. 107933.
- Ikawa, H., Kuwagata, T., Haginoya, S., Ishigooka, Y., Ono, K., Maruyama, A., Sakai, H., Fukuoka, M., Yoshimoto, M., Ishida, S., Chen, C.P., Hasegawa, T., Watanabe, T., 2021. Heat-mitigation effects of irrigated rice-paddy fields under changing atmospheric carbon dioxide based on a coupled atmosphere and crop energy-balance model. Boundary Layer Meteorol. 179 (3), 447–476.
- IPCC, 2019: Climate Change and Land: an IPCC special report on climate change, desertification, land degradation, sustainable land management, food security, and greenhouse gas fluxes in terrestrial ecosystems [P.R. Shukla, J. Skea, E. Calvo Buendia, V. Masson-Delmotte, H.-O. Pörtner, D. C. Roberts, P. Zhai, R. Slade, S. Connors, R. van Diemen, M. Ferrat, E. Haughey, S. Luz, S. Neogi, M. Pathak, J. Petzold, J. Portugal Pereira, P. Vyas, E. Huntley, K. Kissick, M. Belkacemi, J. Malley, (eds.)]. https://www.ipcc.ch/srccl/.
- Jin, K., Wang, F., Zong, Q., Qin, P., Liu, C., 2020. Impact of variations in vegetation on surface air temperature change over the Chinese Loess Plateau. Sci. Total Environ. 716, 136967.
- Kalnay, E., Cai, M.J.N., 2003. Impact of urbanization and land-use change on climate. Nature 423 (6939), 528–531.
- Krishnankutty Ambika, A., Mishra, V., 2019. Observational Evidence of irrigation influence on vegetation health and land surface temperature in India. Geophys. Res. Lett. 46 (22), 13441–13451.
- Lan, X., Li, Y., Shao, R., Chen, X., Lin, K., Cheng, L., Gao, H., Liu, Z., 2020. Vegetation controls on surface energy partitioning and water budget over China. J. Hydrol. 600, 125646.
- Lee, X., Goulden, M.L., Hollinger, D.Y., Barr, A., Black, T.A., Bohrer, G., Bracho, R., Drake, B., Goldstein, A., Gu, L., Katul, G., Kolb, T., Law, B.E., Margolis, H., Meyers, T., Monson, R., Munger, W., Oren, R., Paw U, K.T., Richardson, A.D., Schmid, H.P., Staebler, R., Wofsy, S., Zhao, L., 2011. Observed increase in local cooling effect of deforestation at higher latitudes. Nature 479 (7373), 384–387.
- Liao, W., Rigden, A.J., Li, D., 2018. Attribution of local temperature response to deforestation. J. Geophys. Res. 123 (5), 1572–1587.
- Liu, B., Cui, Y., Luo, Y., Shi, Y., Liu, M., Liu, F., 2019a. Energy partitioning and evapotranspiration over a rotated paddy field in Southern China. Agric. For. Meteorol. 276-277, 107626.
- Liu, J., Zhang, Z., Xu, X., Kuang, W., Zhou, W., Zhang, S., Li, R., Yan, C., Yu, D., Wu, S., Jiang, N., 2010. Spatial patterns and driving forces of land use change in China during the early 21st century. J. Geogr. Sci. 20 (4), 483–494.
- Liu, T., Lingxue, y., Bu, K., Yan, F., Zhang, S., 2018. Seasonal local temperature responses to paddy field expansion from rain-fed farmland in the cold and humid Sanjiang Plain of China. Remote Sens. 10 (12), 2009.

- Liu, T., Yu, L., Zhang, S., 2019b. Impacts of wetland reclamation and paddy field expansion on observed local temperature trends in the Sanjiang Plain of China. J. Geophys. Res. 124 (2), 414–426.
- Liu, X., Zhang, Y., Dong, G., Jiang, M., 2019c. Difference in carbon budget from marshlands to transformed paddy fields in the Sanjiang Plain, Northeast China. Ecol. Eng. 137, 60–64.
- Liu, Z., Ballantyne, A.P., Cooper, L.A., 2019d. Biophysical feedback of global forest fires on surface temperature. Nat. Commun. 10 (1), 214.
- Luo, C., Liu, H.-j., Fu, Q., Guan, H.-x., Ye, Q., Zhang, X.-l., Kong, F.-c., 2020. Mapping the fallowed area of paddy fields on Sanjiang Plain of Northeast China to assist water security assessments. J. Integr. Agric. 19 (7), 1885–1896.
- McNally, A., Arsenault, K., Kumar, S., Shukla, S., Peterson, P., Wang, S., Funk, C., Peters-Lidard, C.D., Verdin, J.P., 2017. A land data assimilation system for sub-Saharan Africa food and water security applications. Sci. Data 4 (1), 170012.
- Moon, M., Li, D., Liao, W., Rigden, A.J., Friedl, M.A., 2020. Modification of surface energy balance during springtime: the relative importance of biophysical and meteorological changes. Agric. For. Meteorol. 284, 107905.
- Nocco, M.A., Smail, R.A., Kucharik, C.J., 2019. Observation of irrigation-induced climate change in the Midwest United States. Glob. Change Biol. 25 (10), 3472–3484.
- Pan, T., Zhang, C., Kuang, W., Luo, G., Du, G., Yin, Z., 2020. Large-scale rain-fed to paddy farmland conversion modified land-surface thermal properties in Cold China. Sci. Total Environ. 722, 137917.
- Peng, S., 2019. High-spatial-resolution monthly temperatures dataset over China during 1901-2017. Earth Syst. Sci. Data 11 (4), 1931–1946.
- Peng, S., Ciais, P., Maignan, F., Li, W., Chang, J., Wang, T., Yue, C., 2017. Sensitivity of land use change emission estimates to historical land use and land cover mapping. Glob. Biogeochem. Cycles 31 (4), 626–643.
- Peng, S., Piao, S., Zeng, Z., Ciais, P., Zhou, L., Li, L., Myneni, R., Yin, Y., Zeng, H., 2014. Afforestation in China cools local land surface temperature. Proc. Natl. Acad. Sci. U. S.A. 111 (8), 2915–2919.
- Prevedello, J.A., Winck, G.R., Weber, M.M., Nichols, E., Sinervo, B., 2019. Impacts of forestation and deforestation on local temperature across the globe. PLoS ONE 14 (3). e0213368.
- Schaaf, C.B., Gao, F., Strahler, A.H., Lucht, W., Li, X., Tsang, T., Strugnell, N.C., Zhang, X., Jin, Y., Muller, J.-P., Lewis, P., Barnsley, M., Hobson, P., Disney, M., Roberts, G., Dunderdale, M., Doll, C., d'Entremont, R.P., Hu, B., Liang, S., Privette, J. L., Roy, D., 2002. First operational BRDF, albedo nadir reflectance products from MODIS. Remote Sens. Environ. 83 (1), 135–148.
- Schwaab, J., Davin, E.L., Bebi, P., Duguay-Tetzlaff, A., Waser, L.T., Haeni, M., Meier, R., 2020. Increasing the broad-leaved tree fraction in European forests mitigates hot temperature extremes. Sci. Rep. 10 (1), 14153.
- Shen, X., Liu, B., Jiang, M., Lu, X., 2020. Marshland loss warms local land surface temperature in China. Geophys. Res. Lett. 47 (6), e2020GL087648.
- Shi, J.-j., Huang, J.-f., Zhang, F., 2013. Multi-year monitoring of paddy rice planting area in Northeast China using MODIS time series data. J. Zhejiang Univ. Sci. B 14 (10), 934–946.
- Singha, M., Dong, J., Sarmah, S., You, N., Zhou, Y., Zhang, G., Doughty, R., Xiao, X., 2020. Identifying floods and flood-affected paddy rice fields in Bangladesh based on Sentinel-1 imagery and Google Earth Engine. ISPRS J. Photogram. Remote Sens. 166, 278–293.
- Song, K., Wang, Z., Du, J., Liu, L., Zeng, L., Ren, C., 2014. Wetland degradation: its driving forces and environmental impacts in the Sanjiang Plain, China. Environ. Manage. 54 (2), 255–271.
- Wang, J., Xiao, X., Zhang, Y., Qin, Y., Doughty, R., Wu, X., Bajgain, R., Du, L., 2018. Enhanced gross primary production and evapotranspiration in juniper encroached grasslands. Glob. Change Biol. 24 (12), 5655–5667.
- Wang, L., Tian, F., Wang, X., Yang, Y., Wei, Z., 2020. Attribution of the land surface temperature response to land-use conversions from bare land. Glob. Planet. Change 193, 103268.
- Wang, Z., Song, K., Ma, W., Ren, C., Zhang, B., Liu, D., Chen, J.M., Song, C., 2011. Loss and fragmentation of marshes in the Sanjiang Plain, Northeast China, 1954–2005. Wetlands 31 (5), 945.
- Wei, D., Wang, X., 2017. Recent climatic changes and wetland expansion turned Tibet into a net CH4 source. Clim. Change 144 (4), 657–670.
- Windisch, M.G., Davin, E.L., Seneviratne, S.I., 2021. Prioritizing forestation based on biogeochemical and local biogeophysical impacts. Nat. Clim. Change 11 (10), 867–871.
- Xiao, X., Boles, S., Liu, J., Zhuang, D., Frolking, S., Li, C., Salas, W., Moore, B., 2005. Mapping paddy rice agriculture in southern China using multi-temporal MODIS images. Remote Sens. Environ. 95 (4), 480–492.
- Xin, F., Xiao, X., Dong, J., Zhang, G., Zhang, Y., Wu, X., Li, X., Zou, Z., Ma, J., Du, G., Doughty, R.B., Zhao, B., Li, B., 2020. Large increases of paddy rice area, gross primary production, and grain production in Northeast China during 2000–2017. Sci. Total Environ. 711, 135183.
- Xu, X., Tang, J., Li, Z., Liu, C., Han, W., 2011. Global warming potential of emissions from rice paddies in Northeastern China. Mitigat. Adapt. Strat. Glob. Change 16 (6), 721–731
- Yan, F., Lingxue, y., Yang, C., Zhang, S., 2018. Paddy field expansion and aggregation since the mid-1950s in a cold region and its possible causes. Remote Sens. 10, 384.
- You, N., Dong, J., 2020. Examining earliest identifiable timing of crops using all available Sentinel 1/2 imagery and Google Earth Engine. ISPRS J. Photogram. Remote Sens. 161, 109–123.
- You, N., Dong, J., Huang, J., Du, G., Zhang, G., He, Y., Yang, T., Di, Y., Xiao, X., 2021. The 10-m crop type maps in Northeast China during 2017–2019. Sci. Data 8 (1), 41.

- Yu, L., Liu, T., 2019. The impact of artificial wetland expansion on local temperature in the growing season—the case study of the Sanjiang Plain, China. Remote Sens. 11 (24), 2915.
- Yu, L., Liu, Y., Liu, T., Yan, F., 2020a. Impact of recent vegetation greening on temperature and precipitation over China. Agric. For. Meteorol. 295, 108197.
- Yu, L., Xue, Y., Diallo, I., 2020b. Vegetation greening in China and its effect on summer regional climate. Sci. Bull. 66 (1), 13–17.
- Yu, W., Zhang, L., Zhang, H., Jiang, L., Zhang, A., Pan, T., 2020c. Effect of farmland expansion on drought over the past century in Songnen Plain, Northeast China. J. Geogr. Sci. 30 (3), 439–454.
- Yuan, X., Hamdi, R., Ochege, F.U., Kurban, A., De Maeyer, P., 2020. The sensitivity of global surface air temperature to vegetation greenness. Int. J. Climatol. 41 (1), 483-496
- Zeng, Z., Piao, S., Li, L.Z.X., Zhou, L., Ciais, P., Wang, T., Li, Y., Lian, X., Wood, E.F., Friedlingstein, P., Mao, J., Estes, L.D., Myneni, R.B., Peng, S., Shi, X., Seneviratne, S. I., Wang, Y., 2017. Climate mitigation from vegetation biophysical feedbacks during the past three decades. Nat. Clim. Change 7 (6), 432–436.
- Zhang, G., Xiao, X., Biradar, C.M., Dong, J., Qin, Y., Menarguez, M.A., Zhou, Y., Zhang, Y., Jin, C., Wang, J., Doughty, R.B., Ding, M., Moore, B., 2017. Spatiotemporal patterns of paddy rice croplands in China and India from 2000 to 2015. Sci. Total Environ. 579, 82–92.

- Zhang, Q., Barnes, M., Benson, M., Burakowski, E., Oishi, A.C., Ouimette, A., Sanders-DeMott, R., Stoy, P.C., Wenzel, M., Xiong, L., Yi, K., Novick, K.A., 2020. Reforestation and surface cooling in temperate zones: mechanisms and implications. Glob. Change Biol. 26 (6), 3384–3401.
- Zhao, G., Dong, J., Cui, Y., Liu, J., Zhai, J., He, T., Zhou, Y., Xiao, X., 2019. Evapotranspiration-dominated biogeophysical warming effect of urbanization in the Beijing-Tianjin-Hebei region, China. Clim. Dyn. 52 (1), 1231–1245.
- Zhao, K., Jackson, R.B., 2016. Biophysical forcings of land-use changes from potential forestry activities in North America. Ecol. Monogr. 84 (2), 329–353.
- Zhao, L., Lee, X., Smith, R.B., Oleson, K., 2014. Strong contributions of local background climate to urban heat islands. Nature 511 (7508), 216–219.
- Zhao, L., Lee, X., Suyker, A., Wen, X., 2015. Influence of Leaf Area Index on the Radiometric Resistance to Heat Transfer. Boundary Layer Meteorol. 158, 105–123.
- Zheng, Y., Dong, L., Xia, Q., Liang, C., Wang, L., Shao, Y., 2020. Effects of revegetation on climate in the Mu Us Sandy Land of China. Sci. Total Environ. 739, 139958.
- Zhou, D., Li, D., Sun, G., Zhang, L., Liu, Y., Hao, L., 2016. Contrasting effects of urbanization and agriculture on surface temperature in eastern China. J. Geophys. Res. 121 (16), 9597–9606.
- Zhou, S., Wang, K., Yang, S., Li, W., Zhang, Y., Zhang, B., Fu, Y., Liu, X., Run, Y., Chubwa, O.G., Zhao, G., Dong, J., Cui, Y., 2020. Warming effort and energy budget difference of various human land use intensity: case study of Beijing, China. Land 9 (9), 280.